Polymer 51 (2010) 3416–3424

Contents lists available at ScienceDirect

Polymer

journal homepage: www.elsevier.com/locate/polymer

Preparation of multifunctional supported metallocene catalyst using organic multifunctional modifier for synthesizing polyethylene/clay nanocomposites via *in situ* intercalative polymerization

Changyi Ren [a,b], Xiaohua Du [a,b], Li Ma [a], Yanhui Wang [a], Jun Zheng [a,b], Tao Tang [a,*]

[a] State Key Laboratory of Polymer Physics and Chemistry, Changchun Institute of Applied Chemistry, Chinese Academy of Sciences, Changchun 130022, China
[b] Graduate School of the Chinese Academy of Sciences, Beijing 100039, China

ARTICLE INFO

Article history:
Received 22 December 2009
Received in revised form
18 May 2010
Accepted 21 May 2010
Available online 1 June 2010

Keywords:
Catalyst
Clay
Nanocomposite

ABSTRACT

A new type of multifunctional ammonium modifier with carbonyl group and vinyl group was synthesized to prepare multifunctional montmorillonites (F-MMTs), which were used as multifunctional catalyst supports for *in situ* ethylene polymerization. High loading of metallocene catalyst in the galleries of F-MMT had been achieved due to the presence of carbonyl group in the multifunctional modifier. XRD profiles and TEM images showed that polyethylene/montmorillonite (PE/F-MMT) nanocomposites with exfoliated structure could be synthesized using the intercalated catalyst described above, even when the content of MMT was very high (more than 15.1 wt%). The as-produced PE/F-MMTs nanocomposites were composed of flower-like particles with a diameter of about 5 μm. A thermal stable monoclinic phase was observed in PE/F-MMT nanocomposites. Comparatively, the resultant PE/F-MMT nanocomposites showed low gas permeability. Interfacial interaction between PE matrix and F-MMT was enhanced due to the chemical linking between the two components via copolymerization of ethylene with vinyl group of F-MMT. Thus the resultant PE/F-MMT nanocomposites showed good structural stability.

1. Introduction

The *in situ* intercalative polymerization for preparing polyolefin/montmorillonite (MMT) nanocomposites is carried out in the presence of an intercalated catalyst within modified MMTs [1–7]. This method has been believed to be more desirable in terms of effectiveness to form nanostructures than solution or melt polymer intercalation assisted by functional polyolefin compatibilizer [8]. In this case, olefin polymerization generally takes place within the interlayer of MMTs. As polyolefin chains grow, the MMT sheets are exfoliated gradually. However, two problems are usually encountered for this method. On one hand, as the driving force for the exfoliation of MMT during *in situ* intercalative polymerization of olefin results from the push force of gradual growing polyolefin chains within the interlayer of MMTs, an adequate amount of catalyst must be fixed in the gallery of MMTs. This depends on how much the catalysts diffuse into the interlayer of MMTs where they should be anchored. Thus organic modification of MMTs is necessary to provide enough interlayer distance for the diffusion of catalysts [3]. There are three routes for fixing catalysts within the interlayer of MMTs, i.e. ion-exchange with cationic metallocene species [9], direct intercalation of catalyst into modified MMTs [3], and supporting with hydroxyl group exposed on the surface of modified MMT sheets via MAO pretreatment [4,7,10,11]. There are plenty of highly reactive structure CH_3—Al— in MAO, which would react with reactive groups such as —O*H or —CO*— to form chemical bond —O*—Al— or —C(CH_3) —O*—Al—; then the catalysts would be supported onto the support via MAO that had been anchored onto the catalyst support. The last method is widely applied; however, most of the hydroxyl groups of MMTs are on the edges, not inside of MMT sheets, mainly leading to the polymerization out of the interlayer of MMT sheets. As a result, the formation of the exfoliated structure is limited, especially when the content of MMTs is high. To resolve this problem, a simple way is to introduce more anchoring sites into the interlayer of MMTs for supporting catalyst, such as hydroxyl group for the supporting of metallocene catalyst [1,5] and $MgCl_2$ for the supporting of Ziegler–Natta catalyst [12]. On the other hand, theoretical studies have showed that simple dispersion of MMTs in polyolefin matrix is thermodynamically unstable in spite of the claimed successes of the *in situ* polymerization method due to immiscibility between polyolefin and clay [1,11,13,14]. Thus polar groups should be included in polyolefin backbones to improve their compatibility with MMTs and enhance the structural stability of nanocomposites formed by *in situ* intercalative

* Corresponding author. Tel.: +86 431 85262004; fax: +86 431 85262827.
E-mail address: ttang@ciac.jl.cn (T. Tang).

0032-3861/$ – see front matter © 2010 Elsevier Ltd. All rights reserved.
doi:10.1016/j.polymer.2010.05.041

polymerization [10]. Alternatively, strong interaction can also be gained by inserting organic modifier into polymer chains [15,16], as organic modifiers for MMTs have strong interaction with MMTs through electrovalent interaction. In this case, functionalized polyolefin itself served as an organic modifier [17].

Therefore, to prepare polyolefin/MMT nanocomposites with exfoliated structure via *in situ* intercalative polymerization, it is requisite to increase the loading of catalyst in the interlayer of MMTs for promoting exfoliation as well as to enhance the interaction in the interface between polyolefin and MMTs for improving the structural stability. Shin et al. used ω-undecylenylalcohol as a polymerizable modifier to modify MMTs in which an intercalated transition metal catalyst was then prepared to synthesize polyethylene (PE)/MMTs nanocomposites [18]. However, the detailed information about modified MMT, intercalated catalyst and copolymerization of ethylene with the polymerizable modifier was not provided. Thus, to date, further exploration for a synthetic method to satisfy the both requirements at the same time is obviously necessary.

Herein, to meet all the needs above simultaneously, we report the design and synthesis of a novel multifunctional MMT (F-MMT) by ion-exchange using a new multifunctional ammonium modifier and the preparation of exfoliated PE nanocomposites based on the F-MMT. This modifier contained carbonyl group and vinyl group besides ammonium group. The carbonyl groups could anchor catalysts within the interlayer of F-MMT, which could also be reduced to hydroxyl group by MAO to increase the structural stability; by *in situ* intercalative polymerization, the vinyl group in the F-MMT could copolymerize with ethylene to strengthen the interaction between PE chains and F-MMT. The microstructures and structural stability of the resultant PE nanocomposites were investigated.

2. Experimental section

2.1. Materials

Na^+-montmorillonites (MMTs) used in this work, with a cation exchange capacity (CEC) of 119 meq/100 g, were from Kunimine Co.. Analytical grade CH_3CN, CH_3COCH_3, K_2CO_3, $Et(OH)_2$, C_2H_5OH, TsOH, Na_2SO_4, *n*-C_6H_{14}, Et_2O, CH_3COOEt, benzene, azobisisbutyronitrile (AIBN), *n*-bromosuccinimide (NBS) and octadecylamine were used without further purification. Carbon tetrachloride (CCl_4) and toluene was dried before use. 4-Methylacetophenone (95% Aldrich), 11-bromo-undecene (95%, Aldrich), *rac*-ethylene bis (4, 5, 6, 7-tetra-hydro-1-indenyl) zirconium dichloride (*rac*-Et$(IndH_4)_2ZrCl_2$, Boulder Scientific Company, marked as Zr-Cat for short), methylaluminoxane (MAO: 10 wt% in toluene, Ethyl Corp.) and ethylene (polymerization grade, Liaoyang Chemical Corp.) were used without further treatment. Undec-10-enylamine was synthesized through Gabriel synthesis method using 11-bromo-undecene, yielding 45%.

2.2. Synthesis

The synthesis route for multifunctional modifier was summarized in Fig. 1a. The preparation of supported catalyst and the *in situ* polymerization of ethylene were summarized in Fig. 1b.

2.2.1. Synthesis of multifunctional modifier (Compound 4 in Fig. 1a)

The precursor Compound 1 was prepared as follow. A solution of 4-methylacetophenone (6.0 g) in dried CCl_4 (150 ml) was added NBS (8.0 g) and AIBN (0.1 g). After the reaction at 65 °C was complete, the solid succinimide, which floats upon the surface, was filtered off and the solvent was removed by a rotary evaporator. The crude product was purified by recrystallization from CH_3COOEt/*n*-C_6H_{14} (6/3, v/v; yielding 42%).

The precursor Compound 2 was prepared as follow. Into a dry 250 ml two-necked flask was transferred benzene (100 ml), followed by Compound 1 (2 g), $Et(OH)_2$ (1 ml) and TsOH (0.02 g). A water separator was equipped on the flask. The mixture was refluxed at 80 °C for 1 day, and the solvent was removed by a rotary evaporator. The crude product was purified by recrystallization from benzene (yielding 85%).

The precursor Compound 3 was prepared as follow. 0.6 g of undec-10-enylamine, 100 ml of CH_3CN and 2.0 g of powder K_2CO_3 were transferred into a dry 250 ml two-necked flask. A condenser was attached and the reaction mixture was placed in an ice bath. 3.8 g of Compound 2 was dissolved in 50 ml of CH_3CN and added into the flask dropwise. After 0.5 h, the temperature was raised up to 35 °C to react for 1 day. After reaction the mixture was filtered, and the filtrate was kept. The crude product was got by evaporating the solvent, and was purified by thin layer chromatography (TLC, silica gel) using a mixed solvent of Et_2O and *n*-C_6H_{14} (1/4, v/v; yielding 53%).

The multifunctional modifier Compound 4 was prepared as follow. A nitrogen-degassed solution of Compound 3 (3 g), TsOH (0.12 g) and H_2O (0.13 g) in CH_3COCH_3 (50 ml) was kept at room-temperature for 3 days. The solvent was removed in vacuo and the residue was partitioned between Et_2O and H_2O. The organic phase

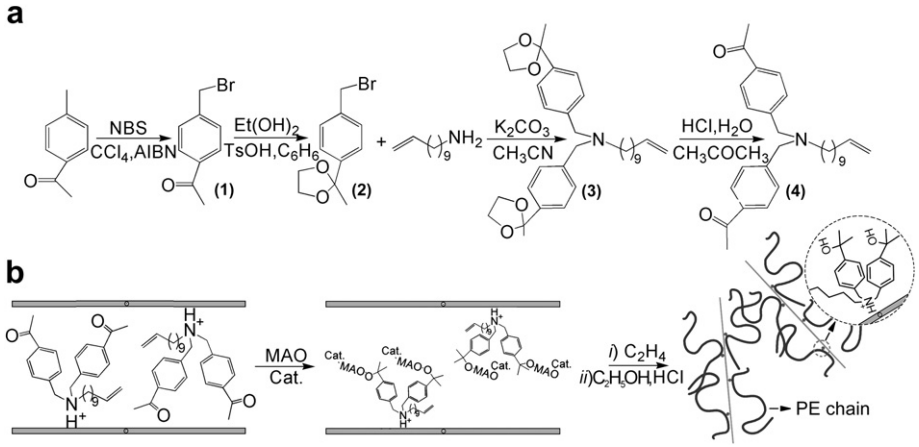

Fig. 1. Synthetic route of multifunctional modifier (Compound 4) (a) and supporting process of catalyst (b).

was kept, and the crude product was got by evaporating the solvent. The multifunctional modifier Compound 4 was purified by thin layer chromatography (TLC, silica gel) using a mixed solvent of Et_2O and n-C_6H_{14} (1/3, v/v; yielding 90%).

2.2.2. Preparation of the multifunctional MMT

The resultant multifunctional modifier was protonated with equal molar concentrated HCl in a mixture solution C_2H_5OH/H_2O (3/7, v/v) at 80 °C via cation exchanging with the interlamellar cations of the MMT. The multifunctional MMT (F-MMT) was got after the sample was washed and freeze-dried.

2.2.3. Preparation of the supported catalysts

A certain amount of F-MMT (0.05–0.40 g) reacted with excess MAO (10 ml) under the protection of Argon for 4 h at 60 °C in toluene in a dried Schlenk-type filtration reactor equipped with a magnetic stirrer. Then the sample was washed with toluene to remove the excess MAO. The resultant sample was named as MAO-F-MMT. It was followed by injecting excess of Zr-Cat solution (1×10^{-3} M, 10–15 ml) and reacting at 60 °C for another 4 h. Then the sample was washed with toluene for three times to get the supported catalyst, named as Zr-F-MMT.

2.2.4. Ethylene polymerization

The resultant catalyst was transferred to a polymerization reactor under protection of Argon. 100 ml of toluene and 3 ml of MAO were added at 60 °C under mechanical stirring, and the polymerization started when ethylene was introduced into the reactor. For different samples, polymerization time changed to get different MMT loading. The polymerization was terminated using acidified ethanol solution; the precipitated product was collected after being washed with ethanol and dried in vacuo at 60 °C for 24 h. For comparison, an octadecylammonium modified MMT (O-MMT) was prepared and the same catalyst was supported on it to perform *in situ* polymerization under the same experimental condition for F-MMT. The supported catalyst was respectively named as Zr-O-MMT. A neat PE sample (HOMO) was also prepared for comparison.

2.3. Characterization

Thermal gravimetric analysis (TGA) was carried out on a Perkin–Elmer TGA-7 Series Thermal Analysis System at a heating rate of 10 °C/min from 50 °C to 700 °C under nitrogen gas. Room-temperature and high-temperature ^{1}H NMR and ^{13}C NMR spectra were recorded on a Bruker AM-400 instrument. Molecular weight and molecular weight distribution of the products were measured with gel permeation chromatography (GPC, PL-GPC-220) operated at 135 °C in 1, 2, 4-trichlorobenzene. Before NMR and GPC measurements, the MMT sheets in PE nanocomposites were removed by dipping them into concentrated HF solution for a week, then washed with ethanol to remove the unreacted modifier and dried. The Zr content of the supported catalysts was determined by inductively coupled plasma atomic emission spectroscopy (ICP) with Plasma-Dec(I) of America Leeman Lab. X-ray photoelectron spectroscopy (XPS) for chemical analysis on a VGESCA Lab MK II was used to investigate the binding energies of the atoms of Zr-Cat and the supported catalyst Zr-F-MMT. Room-temperature and high-temperature wide angle X-ray diffraction (WAXD) were carried out using a Rigaku model D_{max} 2500 with a Cu Kα radiation, and the scanning rate was 5°/min. In the high-temperature WAXD measurement, the temperature rose from 30 °C to 150 °C, and then cooled down to 30 °C; the heating/cooling rate was 5 °C/min, and the data collection time was 6 min per scan. Transmission electron microscope (TEM, JEOL JEM-2010(HR), at 200 kV) was used to investigate the morphology of PE nanocomposites. Field emission scanning electron microscope (FESEM) and energy-dispersive X-ray (EDX) analysis were used to investigate the morphology and the composition of the samples on a XL 30 ESEM FEG scanning electron microscope (Micrio Fei Philips, Holand). Rheological properties were measured on a PHYSICA MCR 300 at 190 °C as a function of angular frequency (ranging from 0.01 to 100 rad/s). The permeation experiments of oxygen through neat PE film and the nanocomposite films were measured with a gas transmission rate (G.T.R.) measurement apparatus (K-315-N-03) at 30 °C. The thickness of the samples was about 30 μm.

3. Results and discussion

Fig. 2 shows the ^{1}H NMR spectra of Compound 4 in $CDCl_3$-d_1. The protons corresponding to the chemical shifts are marked. It is confirmed that the multifunctional modifier precursor contains one amine group, two carbonyl groups and one vinyl group in its molecular structure (Fig. 2). Using protonated multifunctional modifier, multifunctional MMT (F-MMT) was synthesized via ion-exchange. TGA results showed that F-MMT contained about 31.7 wt % the multifunctional modifier (marked as $wt\%_{FM}$).

Fig. 1b shows the preparation process of PE/F-MMT nanocomposites by *in situ* intercalative polymerization. Here Zr-Cat is supported onto F-MMT (or O-MMT as a control) under the designed experimental conditions to prepare the intercalated catalysts, i.e. Zr-F-MMT (or Zr-O-MMT). According to the measurement of ICP, the Zr content of Zr-F-MMT was 3.1 wt%, which was obviously higher than that of Zr-O-MMT (0.4 wt%). Probably the carbonyl groups within the galleries of F-MMT acted as anchoring sites for MAO and then Zr-Cat during supporting process, which is the reason why the loading of catalyst in the Zr-F-MMT is much higher than that in the Zr-O-MMT. XPS spectra were used to investigate the formation of the supported catalyst (Fig. 3). The first peak of the XPS spectrum of Zr-Cat at 181.4 eV was attributed to the Zr $3d_{5/2}$ binding energy; the second peak at higher binding energy was attributed to the Zr $3d_{3/2}$ binding energy [19]. Owing to the spin-orbit splits ($3d_{5/2}$–$d_{3/2}$), the XPS spectrum of Zr-F-MMT did not show a clear peak of Zr 3d spectral line. The binding energy of the Zr 3d spectral lines and the spin-orbit splits ($3d_{5/2}$–$3d_{3/2}$) in the XPS spectra of supported catalyst would be a function of catalyst preparatory methods. Usually, the spin-orbit ($3d_{5/2}$–$3d_{3/2}$) splits into two sets, but the intensity of $3d_{5/2}$ peak in either set is stronger than that of $3d_{3/2}$ peak. So the peak of Zr $3d_{5/2}$ would be clear due to strong intensity of the peak; but the peak of Zr $3d_{3/2}$ would be hard to tell [19]. According to Fig. 3, the peak of Zr $3d_{5/2}$ showed a rise of 2.4 eV in the binding energy compared to that of Zr-Cat. This indicates that the Zr-Cat was supported on F-MMTs. Furthermore, the supporting process was also confirmed by the XRD data. Fig. 4 shows the XRD profiles of F-MMT, MAO-F-MMT and Zr-F-MMT. The (001) diffraction peak of MMT in the MAO-F-MMT shifted to lower

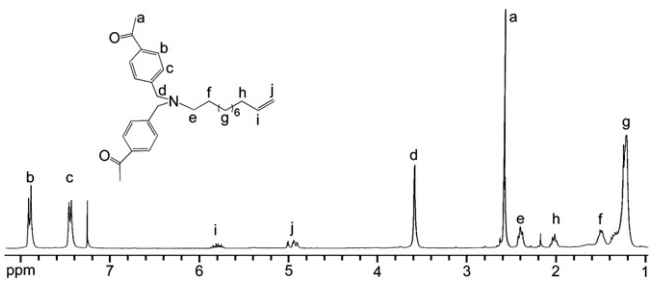

Fig. 2. ^{1}H NMR spectrums of multifunctional modifier Compound 4 in $CDCl_3$-d_1.

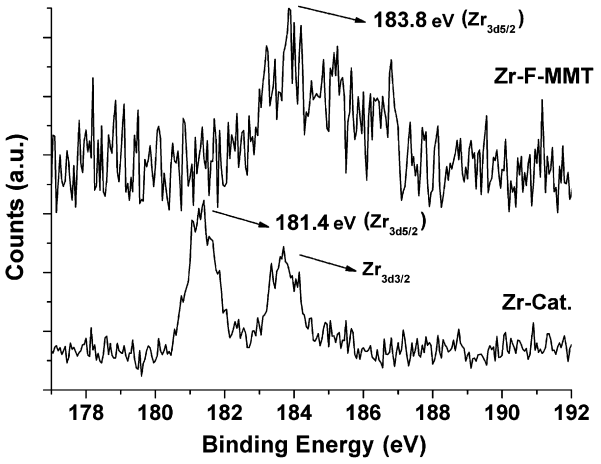

Fig. 3. XPS spectra of Zr-F-MMT and Zr-Cat.

angle as compared to that of F-MMT, indicating that MAO has intercalated into the gallery of F-MMT; the (001) diffraction peak of MMT in the Zr-F-MMT shifted to lower angle as compared to that of MAO-F-MMT, indicating that the Zr-Cat has been supported in the gallery of MAO-F-MMT.

Table 1 shows the polymerization results. Six samples included one neat PE (HOMO) from homogeneous catalyst, four PE/F-MMT nanocomposites (F1–F4) from the intercalated catalyst Zr-F-MMT and one PE/O-MMT nanocomposite (O1) from the intercalated catalyst Zr-O-MMT. The results showed that the catalytic activities of all the supported catalysts were lower than that of homogeneous catalyst, but the catalytic activity of Zr-F-MMT per gram of supported catalyst was much higher than that of Zr-O-MMT. Compared to HOMO sample and O1, the molecular weight of PE in the PE/F-MMT nanocomposites was low due to copolymerization, which is similar to the results of copolymerization of ethylene with α-olefin [20,21].

Fig. 4 also presents the XRD profiles of F2, F3 and O1 samples. Very strikingly, at the high content of F-MMTs (sample F3, 15.1 wt %), the (001) diffraction peak of MMT disappeared, meaning that F-MMT is completely exfoliated in PE matrix, without saying F2 (8.0 wt%) and F1 (3.7 wt%; XRD profile, similar to that of F2 and F3,

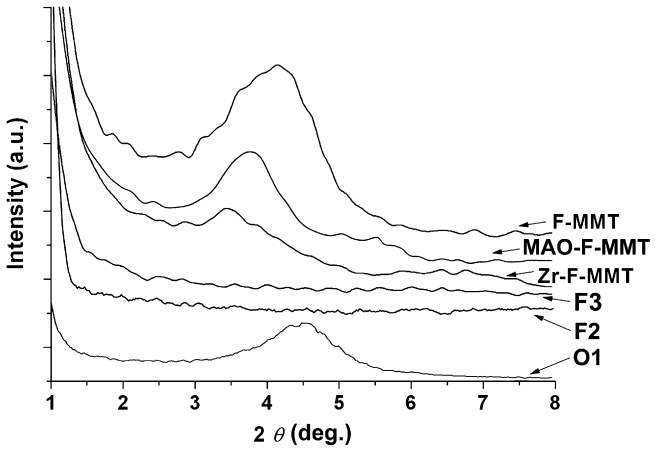

Fig. 4. XRD profiles of organic modified MMT (F-MMT), MAO treated F-MMTs (MAO-F-MMT), catalyst supported MMT (Zr-F-MMT) and PE/MMT nanocomposite F2 (8.0 wt% F-MMT), F3 (15.1 wt% F-MMT) and O1 (8.2 wt% O-MMT) gained by *in situ* polymerization.

Table 1
Results of ethylene polymerization catalyzed by intercalated catalysts.

Sample[a]	MMT[b]	Activity	M_w	PDI
	wt%	10^{-6} g PE atm^{-1} h^{-1}·(mol Zr)$^{-1}$	10^4[c]	
HOMO	Null	2.20	22.7	2.7
F1	3.7	0.83 (278)[d]	13.2	3.0
F2	8.0	0.80 (268)	13.0	2.9
F3	15.1	0.79 (264)	12.0	3.2
F4	17.7	0.84 (280)	12.2	2.8
O1	8.2	0.71 (31)	20.6	2.8

[a] Other conditions: 0.1 MPa ethylene, 100 ml toluene, 3 ml MAO, temperature = 60 °C.
[b] Measured by TGA analysis.
[c] Measured by GPC, the samples containing MMTs was dipped in HF to remove MMT before examine.
[d] The parentheses were the activities of supported catalyst: g PE atm^{-1} h^{-1}·(g supported catalyst)$^{-1}$.

was not listed). But there was still a clear peak of O-MMT for O1, indicating that the O-MMT is not completely exfoliated. This may be due to the low Zr-Cat loading of Zr-O-MMT. TEM images further proved that both F1 and F3 were of exfoliated structure (Fig. 5a and b), but O1 was not in spite of a low loading of MMT compared with F3 (Fig. 5d). In the high-magnification TEM image of F3, individual MMT sheets could be observed clearly (Fig. 5c). Comparatively, without the effective intercalation of enough amount of Zr-Cat into the interlayer of MMT, such as in the case of O-MMT, the large aggregates of MMT sheets were observed in the O1 sample. These results confirm that it is necessary to introduce the high amount of Zr-Cat into the interlayer of MMT in the preparation of PE/MMT nanocomposites via *in situ* intercalative polymerization.

Very surprisingly, the nascent morphologies of both F2 and O1 showed different superstructures although both the samples contained the same content of MMT (Fig. 6). The as-produced nanocomposite of F2 was composed of flower-like particles with a diameter of about 5 μm (Fig. 6a), in which there were many layer structures (Fig. 6b). In contrast, the nascent morphology of O1 was of aggregated particles (Fig. 6c), and no flower-like structures were observed (Fig. 6d). This may result from the dispersion of organic modified MMT and the "morphology duplicating effect" of supported catalyst [22]. The organoclay would swell in the organic media at different scales, i.e., interplatelet swelling at nanoscopic scale; swelling at the microscopic scale to form spherical gels by percolation of microgels, based on swollen 3–4 platelet tactoids [23]. In the case of Zr-F-MMT, more Zr-Cat was supported within the galleries of MMT. Thus almost each Zr-F-MMT sheet served as the catalyst supporter, and the resultant PE duplicated the morphology of Zr-F-MMT sheet to form a layer structure. At the same time, Zr-F-MMT was swelling at the microscopic scale to form spherical gels in toluene; so the as-produced PE/F-MMT nanocomposite was composed of spherical flower-like particles. However, in the case of Zr-O-MMT, the loading of Zr-Cat within the gallery of MMT is low, so Zr-O-MMT tactoids would serve as the catalyst supporter. As a result, the resultant PE duplicated the morphology of Zr-O-MMT tactoids to form solid particles. In this case, MMT platelets are not completely exfoliated during ethylene polymerization. The detailed formation process for the formation of the flower-like particles needs to be further investigated. A similar superstructure was observed in the F3 (Fig. 7). The as-produced nanocomposite was also composed of flower-like particles with a diameter of about 5 μm, in which there are many layer structures (Fig. 7b). EDX image showed a homogeneous dispersion of Si element on the as-produced particles of F3 (Fig. 7d), which further confirms the homogeneous dispersion of MMT sheets in the F3 sample.

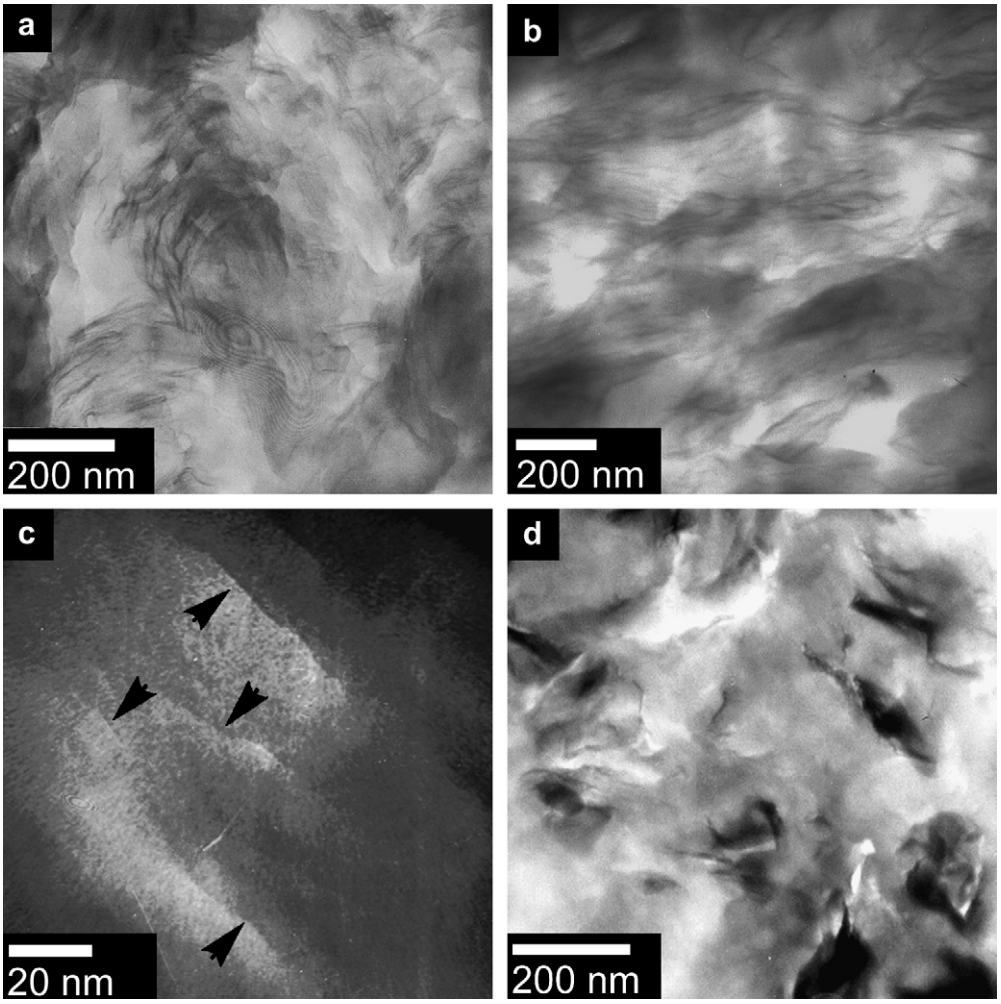

Fig. 5. TEM images of PE nanocomposites. (a) F1; (b) F3; (c) TEM image of F3 at high-magnification, individual F-MMT sheets were marked by arrows; (d) O1.

Fig. 8 shows the WAXD patterns of as-produced O1, F2 and F3. The arrows were used to mark the reflections of the nanocomposites. Very interestingly, (110) and (200) orthorhombic reflections were found in the patterns of F2 and F3, which are typical reflections of PE matrix, meanwhile (010) monoclinic reflection was also observed. It is well-known that the stable orthorhombic phase of PE can be transformed into the metastable monoclinic phase by stress [24,25]. This process is called martensitic transformation. In the *in situ* intercalative polymerization for preparing PE/MMT nanocomposites, it is believed that the exfoliation of MMT platelets are driven by the stress, which should be formed *in situ* when more and more PE chains are synthesized in the limited space of intergalleries of MMTs. There were other reports that monoclinic crystals were formed in the PE sample synthesized by using heterogeneous catalysts [26,27]. The presence of monoclinic crystals was believed to be consistent with a deformation process, arising from impingement of growing polymer particles [26]. The concentration of monoclinic crystals could be increased when α-olefin was introduced in the PE backbone by copolymerization, as the side chain of the resultant PE would disturb the crystallization of orthorhombic phase to form more monoclinic crystals [27]. This may be another reason that monoclinic phase was found in PE/F-MMT nanocomposites, as the multifunctional modifiers would be proved to be involved in the PE backbone by copolymerization in following discussion. But the WAXD pattern of as-produced O1 did not have the (010) monoclinic reflection. This indicates that ethylene polymerization in the gallery of F-MMTs should be more drastic than in the gallery of O-MMT, which is caused by the significant difference in the catalyst loading of both F-MMTs and O-MMTs. High-temperature WAXD was used to further investigate this phenomenon (Fig. 9). As mentioned, the monoclinic phase is metastable, usually it can be eliminated by thermal treatments. In the high-temperature WAXD measurements, F2 was heated up to 150 °C then cooled down to 30 °C. The reflection peaks were slightly shifted to lower degree when the temperature rose, which is due to the expansion of the crystalline cell. Surprisingly, the peak of (010) monoclinic reflection could be still observed after the heat treatment. The reason for that is not clear. It may be due to the high content and good dispersion of F-MMT platelets, which hinder the crystallites from reorganization [28].

Besides increasing the catalyst loading, the formation of chemical linking between PE matrix and MMTs in PE/F-MMT nanocomposites was the other important intention using the multifunctional modifier to modify MMTs. The sample F4 with the highest loading of MMT (17.7 wt%) was used for NMR characterization, considering the insensitive of NMR analysis to the moieties of low concentration. Fig. 10 shows the ^{1}H NMR (a) and ^{13}C NMR (b) spectra of F4 (after HF treatment) in 1,1,2,2-tetrachloroethane-d_2 at 130 °C. The chemical shifts and their corresponding structures were

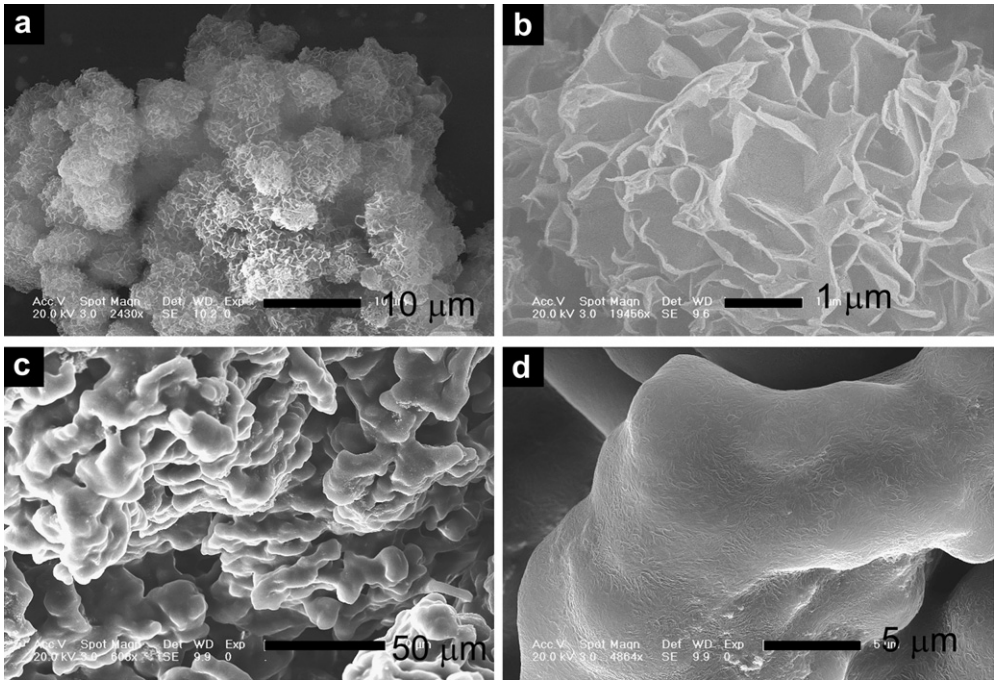

Fig. 6. FESEM images of as-produced F2 (a, b) and O1 (c, d) at low-magnification and high-magnification.

marked in the spectra. In Fig. 10a, the chemical shift at $\delta = 7.16$ ppm represents the characteristic resonance for the marked proton *d*. In Fig. 10b, the chemical shifts at $\delta = 146.7$ ppm, $\delta = 131.5$ ppm, $\delta = 128.3$ ppm and $\delta = 118.1$ ppm represent the characteristic resonance for the marked carbon *b*, *e*, *d* and *c*, respectively. These results mean that the modifier molecule has been inserted into PE backbone. By theoretical calculation and simulation, the change of chemical shift indicates that the carbonyl groups on the multi-functional modifier were reduced to hydroxyl group by MAO, confirming that carbonyl groups act as the anchoring sites for MAO and then Zr-Cat during supporting process. Furthermore, by calculation using the integral intensity of ^{1}H NMR peaks, GPC and other available data, more detailed information about copolymerization of ethylene with F-MMT could be evaluated, including the weight percentage of the modifier linked to PE backbone (wt $\%_{FM-PE}$), the molar percentage of reacted modifier molecules (R_{CM}), the number of the modifier molecules (from each MMT sheet) linked to PE backbone (N_{FM-MMT}), the number of the modifier

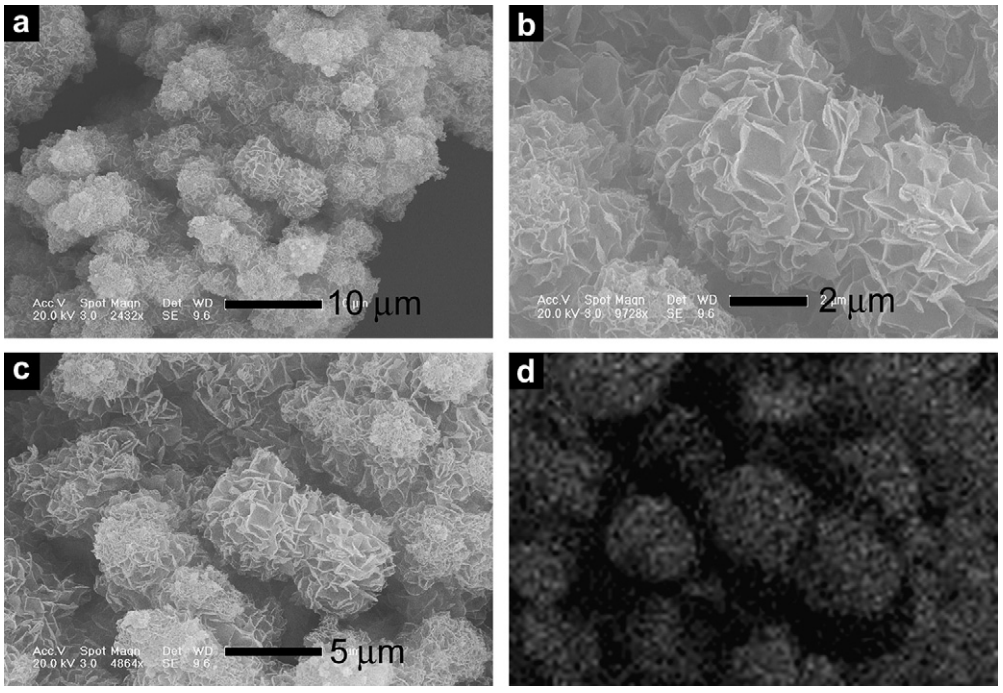

Fig. 7. FESEM images of as-produced F3 at low-magnification (a) and high-magnification (b) and EDX image of Si element (d) corresponding to image (c).

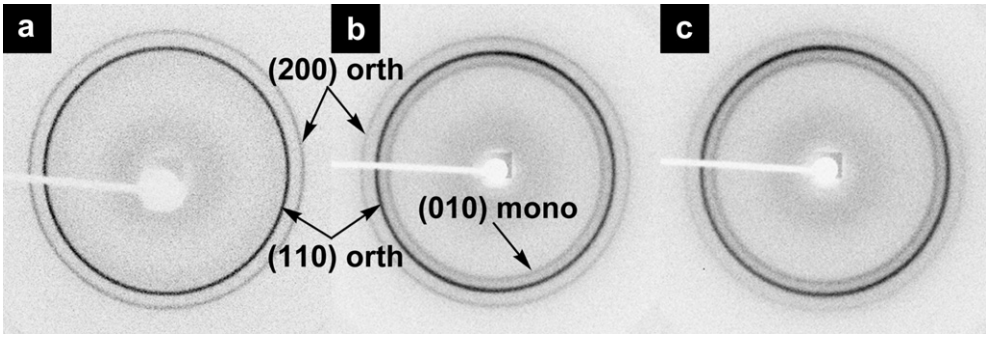

Fig. 8. WAXD patterns of as-produced O1 (a), F2 (b) and F3 (c); the arrows marked the (110), (200) orthorhombic reflections and (010) monoclinic reflection of PE.

molecules linked to each PE chain (N_{FM-PE}), and the number of PE chains linked to each MMT sheet (N_{PE-MMT}). They could be calculated by Equations (1)–(5):

$$wt\%_{FM-PE} = \frac{M_{FM} \times I_{FM}/4}{M_{FM} \times I_{FM}/4 + M_{CH_2} I_{PE}/2} \quad (1)$$

$$R_{CM} = \frac{(1 - wt\%_{F-MMT}) \times wt\%_{FM-PE}}{wt\%_{F-MMT} \times wt\%_{FM}} \quad (2)$$

$$N_{FM-MMT} = \frac{R_{FM} \times NA \times wt\%_{FM}/(1 - wt\%_{FM})}{M_{FM} A_{MMT}/A_{sheet}} \quad (3)$$

$$N_{FM-PE} = \frac{wt\%_{FM-PE}/M_{FM}}{1/M_{nPE}} \quad (4)$$

$$N_{PE-MMT} = \frac{N_{FM-MMT}}{N_{FM-PE}} \quad (5)$$

Here M_{FM} represents the molecular weight of the multifunctional modifier, M_{CH_2} represents the molecular weight of methylene unit (CH_2) in PE backbone. I_{FM} and I_{PE} are the integral intensities at the chemical shifts corresponding to proton *ii* and PE backbone on the ^{1}H NMR spectrum, respectively. They are 1 and 1038 according to Fig. 10. $wt\%_{FM}$ represents the weight percentage of the multifunctional modifier in the F-MMT, which is 31.7 wt%. $wt\%_{F-MMT}$ represents the MMT content of the sample, here it is 17.7 wt% for F4. A_{MMT} is the surface area of MMT, it is believed to be 700–800 m^2/g [29]. *NA* represents the Avogadro constant. A_{sheet} represents the surface area of each sheet of MMT. Supposing the shape of MMTs is round, then $A_{sheet} = 2\pi d^2/4$, and because the aspect of used MMTs is 100–200, hence d (diameter of each sheet) could be 100–200 nm. The average values of A_{MMT} and d are taken, i.e. 750 m^2/g and 150 nm respectively. M_{nPE} is the number-average molecular weight of PE, which could be calculated by M_w and PDI in Table 1. By calculation, it turns out that $wt\%_{FM-PE}$ = 1.6 wt%, R_{CM} = 23.5 wt%, N_{FM-MMT} = 2110, N_{FM-PE} = 1.8, and N_{PE-MMT} = 1172. As it is well-known that naturally occurring layered silicates (such as MMTs) are inhomogeneous across layers [30], these results only fit for the case of F4. Hence such calculations serve only as an approximate guide to the copolymerization efficiency in the PE/F-MMT nanocomposites.

The chemical linking provides the strong interfacial interaction and good compatibility between PE matrix and F-MMTs. Extraction experiment was performed to demonstrate the interfacial interaction between PE matrix and MMTs in the PE/F-MMT nanocomposites. Fig. 11 shows the EDX patterns of F2 and O1 after extraction using boiling decalin, and the insets are the corresponding FESEM images. According to the EDX patterns, a large amount of PE remained in the case of F2 after extraction for 48 h; by contraries, only a trace amount of PE remained in the case of O1.

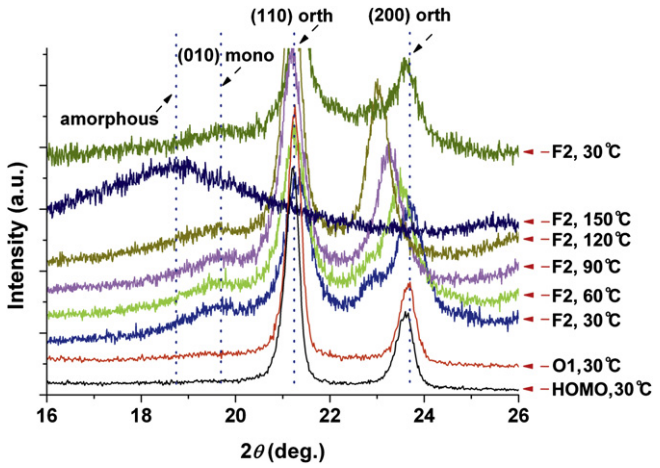

Fig. 9. High-temperature WAXD patterns of F2 (the temperature raised from 30 °C to 150 °C then cooled down to 30 °C, and the heating/cooling rate was 5 °C/min).

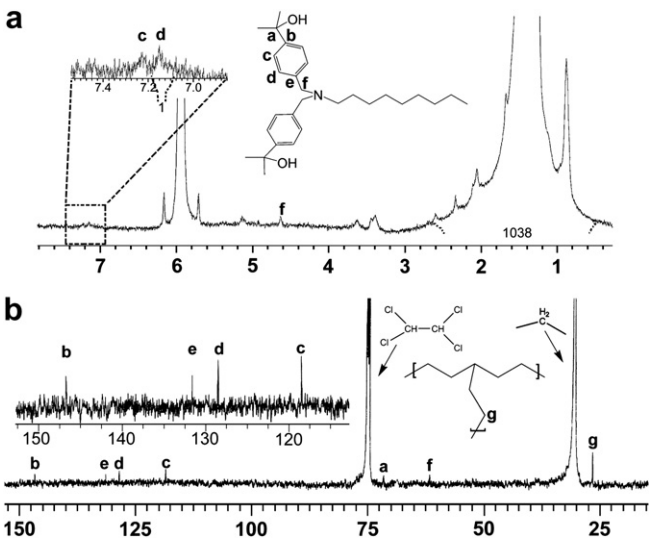

Fig. 10. ^{1}H NMR (a) and ^{13}C NMR (b) spectrum of concentrated HF treated F4 (17.7 wt% MMT) in 1,1,2,2 -tetrachloroethane-d_2 at 130 °C; the chemical shifts and their corresponding structure are marked.

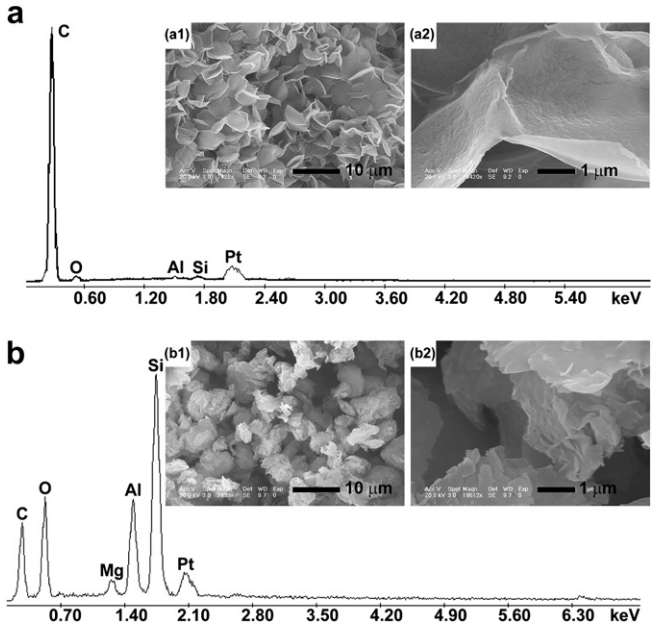

Fig. 11. (a) EDX pattern of F2 after extracting pure PE with boiling decalin for 48 h (corresponding to the area shown in the FESEM image a1), the insets are FESEM micrographs of F2 after solvent extraction at low-magnification (a1) and high-magnification (a2); (b) EDX pattern of O1 after extracting pure PE with boiling decalin for 48 h (corresponding to the area shown in the FESEM image b1), the insets are FESEM micrographs of O1 after solvent extraction at low-magnification (b1) and high-magnification (b2).

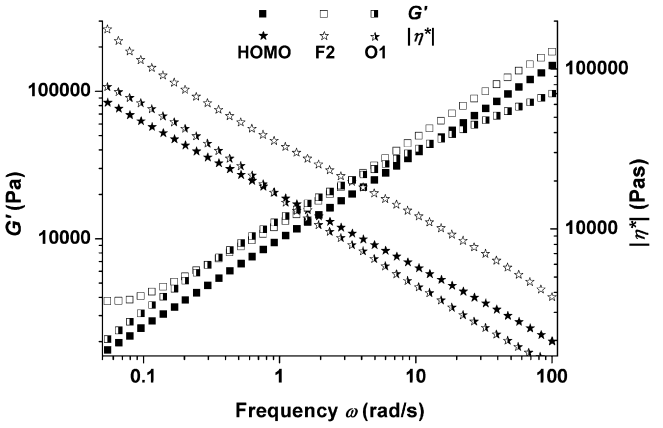

Fig. 12. Plots of log G', G'' and $|\eta^*|$ vs. log ω for HOMO, F2 and O1 at 190 °C.

This indicates significant difference in the interfacial interaction between the two samples. As expected, the dispersion states of F2 and O1 in hot xylene at 135 °C were different. The system of F2 showed a homogeneous dispersion in hot xylene, confirming that the MMT sheets in the F2 could be stably dispersed in hot xylene. This is because some PE chains were anchored to the MMT sheets by copolymerization of ethylene with the copolymerizable vinyl on the modifier molecule. In contrast, the MMTs in the O1 system had deposited on the bottom because of no direct connection between PE and MMT sheets. The difference in the dispersion states of F2 and O1 in hot xylene clearly confirms that the copolymerization between F-MMT and ethylene should be carried out in the sample of F2.

Rheological analysis further confirmed the above conclusion. Generally the linear viscoelastic response of a nanocomposite melt is strongly influenced by the factors, such as dispersion state of particle, inter-particle and particle–polymer interactions. Fig. 12 shows the plots of storage modulus (G') and complex viscosity ($|\eta^*|$) versus frequency (ω) for the PE/MMT nanocomposites. O1 and HOMO show a nearly liner response in the plots of log $|\eta^*|$ vs log ω because of the existence of long chain branch [31,32], which were produced via the insertion of vinyl-terminated PE formed *in situ* through β-hydride elimination or chain transfer to the monomer [33–35]. In the case of F2, the presence of F-MMTs significantly changed this behavior, especially in the low-frequency region. The G' and $|\eta^*|$ of F2 at low frequencies were much higher than those of O1. More importantly, a strong tendency of G' to plateau and a significant $|\eta^*|$ upturn at low-frequency regime was observed in the F2, which is widely accepted as the evidence of a network-like structure and strong interfacial interaction [29,32,36–42].

PE is a typical polymer in the film application, but its barrier property is poor. Adding clay into the PE matrix to form a PE/clay nanocomposite is a promising method to reduce the gas permeability of PE. However, the gas permeability of a polymer/clay nanocomposite depends on the dispersion degree and the orientation degree of the clay platelets in the polymer matrix. In this work, there was no orientation of clay in PE/F-MMT and PE/O-MMT nanocomposites. Therefore the gas permeability only depends on the dispersion degree of clay platelets. The permeability coefficients of oxygen for HOMO, O1 (8.2 wt% O-MMT) and F2 (8. F-MMT) at 30 °C are listed in Table 2. Compared to pristine PE (HOMO), the gas permeabilities of O1 and F2 were reduced 67% and 85%, respectively. The difference demonstrated that the exfoliation degree of clay platelets in the F2 was much higher than that in the O1. PE/F-MMT nanocomposites with low gas permeability are potential in the application, such as food and beverage package, etc.

Annealing experiments via compression molding at high-temperature were used to monitor the structural stability of the resultant nanocomposites. After annealing at 170 °C for 20 min, both WAXD profiles and TEM images showed that the exfoliated structures were still kept in the F1 and F2 comparing with those of original samples (Fig. 13). This proves that PE/F-MMT nanocomposites have the good structural stability even at high-temperature. The main reason for the good structural stability results from the formation of strong interfacial interaction between PE chains and MMT sheets due to chemical linking of some PE chains to the modifier molecules in the F-MMTs. In the PE/F-MMT nanocomposites, the modifier molecules incorporated into PE chains act as a bridge. They have strong interaction with PE chains via covalent bonding and with MMT sheets via electrovalent interaction. Additionally, according to the ^{1}H NMR analysis of model reaction between MAO and the modifier precursor, the carbonyl groups could be reduced to hydroxyl group, which could further enhance the interaction between the modifier molecules and the surface of MMT sheets. As a result, the structural stability of PE/F-MMT nanocomposites can be further improved.

Table 2
The permeability coefficient of oxygen for the samples at 30 °C.

Sample	HOMO	O1	F2
MMTs content (wt%)	0	8.2	8.0
Transmission rate (barrer[a])	6.15	2.02	0.95
P_n/P_h[b]	1	0.33	0.15

[a] 1 barrer = 10^{-10} cm cm^3 cm^{-2} s cmHg.
[b] P_h: oxygen transmission rate of the HOMO sample; P_n: oxygen transmission rate of the nanocomposite sample.

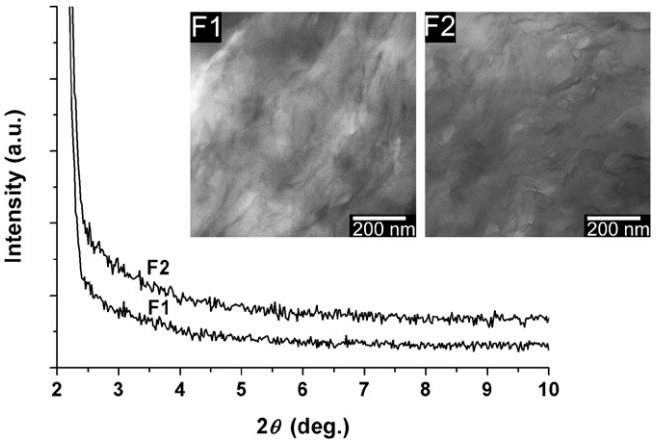

Fig. 13. XRD profiles and TEM images of F1 and F2 samples after annealing at 170 °C for 20 min.

4. Conclusions

We demonstrated an efficient *in situ* intercalative polymerization method for synthesizing exfoliated PE/MMT nanocomposites with good structural stability. This was on the basis of using the multifunctional ammonium modifier bringing carbonyl group and vinyl group. The F-MMT, originated from modifying MMT by the multifunctional modifier, could anchor more the metallocene catalyst within the gallery of MMT due to the presence of carbonyl group in the F-MMT. In this case, more PE chains could be formed in the interlayer of F-MMT during the *in situ* intercalative polymerization, which leads to the formation of more exfoliated structure in the resultant products, even at high content of F-MMT. The as-produced PE/F-MMTs nanocomposites were composed of flower-like particles with a diameter of about 5 μm. The formation of a thermal stable monoclinic phase in PE/F-MMT nanocomposites probably resulted from the stress formed during the polymerization and the copolymerization of the multifunctional modifier with ethylene. Moreover, some of PE chains in PE/F-MMT nanocomposites were chemically linked to the surface of F-MMT sheets through the vinyl group of the multifunctional modifier during ethylene polymerization. Therefore there was strong interaction between MMT sheets and polymer matrix, which could stabilize the microstructure of the nanocomposites during processing at high-temperature. We believed that the above method will shed a light on the further exploration of preparing polymer/MMT nanocomposites with exfoliated structure and good structural stability, especially with special aggregate states of nascent particles, such as flower-like particles.

Acknowledgements

We thank the financial supports from the National Natural Science Foundation of China for the Outstanding Youth Project (no. 50525311), Key Project (20734006) and the Fund for Creative Research Groups (no. 50921062).

References

[1] Jin YH, Park HJ, Im SS, Kwak SY, Kwak S. Macromol Rapid Commun 2002;23:135.
[2] Sun T, Garces JM. Adv Mater 2002;14:128.
[3] Bergman JS, Chen H, Giannelis EP, Thomas MG, Coates GW. Chem Commun 1999;21:2179.
[4] Lee DH, Kim HS, Yoon KB, Min KE, Seo KH, Noh SK. Sci Technol Adv Mater 2005;6:457.
[5] Wei L, Tang T, Huang B. J Polym Sci Part A: Polym Chem 2004;42:941.
[6] Liu C, Tang T, Wang D, Huang B. J Polym Sci Part A: Polym Chem 2003;41:2187.
[7] Ray S, Galgali G, Lele A, Sivaram S. J Polym Sci Part A: Polym Chem 2005;43:304.
[8] Heinemann J, Reichert P, Thomann R, Mulhaupt R. Macromol Rapid Commun 1999;20:423.
[9] Tudor J, Willington L, O'Hare D, Royan B. Chem Commun 1996;17:2031.
[10] Huang Y, Yang K, Dong JY. Macromol Rapid Commun 2006;27:1278.
[11] Alexandre M, Dubois P, Sun T, Garces JM, Jerome R. Polymer 2002;43:2123.
[12] Du K, He AH, Liu X, Han CC. Macromol Rapid Commun 2007;28:2294.
[13] Vaia RA, Giannelis EP. Macromolecules 1997;30:7990.
[14] Balazs AC, Singh C, Zhulina E, Lyatskaya YL. Acc Chem Res 1999;32:651.
[15] Barus S, Zanetti M, Lazzari M, Costa L. Polymer 2009;50:2595.
[16] Wang WS, Chen HS, Wu YW, Tsai TY, Chen-Yang YW. Polymer 2008;49:4826.
[17] Wang ZM, Nakajima H, Manias E, Chung TC. Macromolecules 2003;36:8919.
[18] Shin SYA, Simon LC, Soares JBP, Scholz G. Polymer 2003;44:5317.
[19] Atiqullah M, Faiz M, Akhtar MN, Salim MA, Ahmed S, Khan JH. Surf Interface Anal 1999;27:728.
[20] Grieken R, Martín C, Moreno J, Prieto O, Bravo JM. Macromol Symp 2007;259:174.
[21] Hammawa H, Wanke SE. Polym Int 2006;55:426.
[22] Galli P, Luciani L, Cecchin G. Angew Makromol Chem 1981;94:63.
[23] Burgentzlé D, Duchet J, Gérard JF, Jupin A, Fillon B. J Colloid Interf Sci 2004;278:26.
[24] Russell KE, Hunter BK, Heyding RD. Polymer 1997;38:1409.
[25] Butler MF, Donald AM, Bras W, Mant GR, Derbyshire GE, Ryan AJ. Macromolecules 1995;28:6383.
[26] Ottani S, Wagner BE, Poter RS. Polym Commun 1990;13:370.
[27] Benn R, Fink G, Herrmann W, Müller T. Makromol Chem Rapid Commun 1992;13:321.
[28] Chiu F-C, Fu S-W, Chuang W-T, Sheu H-S. Polymer 2008;49:1015.
[29] Lee KM, Han CD. Macromolecules 2003;36:7165.
[30] Krishnamoorti R, Giannelis EP. Macromolecules 1997;30:4097.
[31] Lohse DJ, Milner ST, Fetters LJ, Xenidou M, Hadjichristidis N, Mendelson RA, et al. Macromolecules 2002;35:3066.
[32] Ye Z, AlObaidi F, Zhu S. Ind Eng Chem Res 2004;43:2860.
[33] Wang WJ, Yan D, Zhu S, Hamielec AE. Macromolecules 1998;31:8677.
[34] Kolodka E, Wang WJ, Zhu S, Hamielec AE. J Appl Polym Sci 2004;92:307.
[35] Stapleton RA, Chai J, Nuanthanom A, Flisak Z, Nele M, Ziegler T, et al. Macromolecules 2007;40:2993.
[36] Goharpey F, Nazockdast H, Katbab AA. Polym Eng Sci 2005;45:84.
[37] Tang CY, Xiang LX, Su JX, Wang K, Yang CY, Zhang Q, et al. J Phys Chem B 2008;112:3876.
[38] Kashiwagi T, Du FM, Douglas JF, Winey KI, Harris RH, Shields JR. Nat Mater 2005;4:928.
[39] Kharchenko SB, Douglas JF, Obrzut J, Grulke EA, Milger KB. Nat Mater 2004;3:564.
[40] Du F, Scogna RC, Zhou W, Brand S, Fischer JE, Winey KI. Macromolecules 2004;37:9048.
[41] Cipriano BH, Kota AK, Gershon AL, Laskowski CJ, Kashiwagi T, Bruck HA, et al. Polymer 2008;49:4846.
[42] Filippone G, Dintcheva NT, Acierno D, La Mantia EP. Polymer 2008;49:1312.